Journal of Geophysical Research: Solid Earth

Supporting Information for

Frictional and Hydraulic Properties of Plate Interfaces Constrained by a Tidal Response Model Considering Dilatancy/Compaction

Ryunosuke Sakamoto[1] and Yoshiyuki Tanaka[2]

[1]Department of Earth and Space Science, Osaka University, Osaka, Japan

[2]Department of Earth and Planetary Science, The University of Tokyo, Tokyo, Japan

Contents of this file

Text S1, S2, S3 and S4

Figures S1, S2, S3, S4, S5 S6, S7 and S8

Introduction

TextS1 presents the governing equation of the drained model.

TextS2 presents the nondimensionalized governing equation of the drained model.

TextS3 presents a numerical method for solving the governing equation of the drained model.

TextS4 presents the approximate solution for the tidal response of the drained model.

Figure S1 shows a schematic of the undrained and drained models.

Figure S2 shows the numerical solution of c in equation (12) for the undrained model.

Figure S3 shows the numerical and approximate solutions for the tidal responses α and δ of the drained model.

Figure S4 shows the numerical solution of c in equation (12) for the drained model.

Figure S5 shows the time variation of the tidal Coulomb stress term ($\Delta S(t)$ of equation (21)), the dilatancy/compaction effect term and the evolution effect term in equation (21).

Figure S6 shows a schematic illustration of the relationship between the fault creep velocity and the tide level when $U = 1$.

Figure S7 shows the dependence of the parameter E_p on the phase difference.

Figure S8 shows the dependence of d_c on the tidal sensitivity and phase difference when $V_{pl} = 10^{-7}$ and 10^{-9} m/s.

Text S1. Derivation of the governing equations for the drained model

We explain a drained model in which pore fluids flow out of the shear zone (Figure S1b). The difference between the undrained and drained models is the presence of fluid flow. The governing equations of the drained model are the same as those in the undrained model (equations (3), (4) and (8)), except for the governing equation for pore fluids.

Following the work of Segall et al. (2010), we assume homogeneous diffusion (HD), which holds under the condition that $T \gg t_w$. In the HD case, the effect of the finite shear zone thickness can be neglected, so the width of the shear zone can be formally defined as $w \to 0$ (Segall et al., 2010). The direction of fluid flow (Figure S1b) is parallel to the z-axis, and the

shear zone lies on $z = 0$. c_{hyd} denotes the fluid pressure diffusivity at $z \neq 0$. Then, the governing equation for pore fluids can be written as (Segall et al., 2010)

$$\frac{\partial p}{\partial t} = c_{hyd} \frac{\partial^2 p}{\partial z^2} \quad \left(\left. \frac{\partial p}{\partial z} \right|_{z=0} = \frac{M w \dot{\phi}}{2 c_{hyd}} \right). \tag{S1}$$

Text S2. Nondimensionalization of the governing equations of the drained model

The governing equations for the drained model are the upper three in equation (10) and the nondimensionalized equation (S1). When we adopt $\sqrt{c_{hyd} T}$ as the representative length in the z-axis direction, the nondimensionalized equation (S1) can be written as

$$\frac{\partial \tilde{p}}{\partial \tilde{t}} = \frac{\partial^2 \tilde{p}}{\partial \tilde{z}^2} \quad \left(\left. \frac{\partial \tilde{p}}{\partial \tilde{z}} \right|_{\tilde{z}=0} = -E_p \frac{1}{\tilde{\theta}} \frac{d\tilde{\theta}}{d\tilde{t}} \right), \tag{S2}$$

where $E_p = M\epsilon / 2\sigma_{eff}^0 \sqrt{w^2 / T c_{hyd}} = U/2 \sqrt{w^2 / T c_{hyd}}$. E_p represents the relative importance of the dilatancy/compaction effect to the effective normal stress change in the drained model. Previous experiments and observations suggest that $c_{hyd} \sim 10^{-1\sim3}$ $\mathrm{m^2/s}$ (Yamashita and Tsutsumi, 2018) and $U \sim 10^{0\sim-2}$ (Section 2.2.3). Using $10^{0\sim1/2}$ m as the value of w (Section 4.3.4), we obtain a possible range of E_p as 10^{-2} to 10^{-4}.

Text S3. A numerical method for solving the governing equation of the drained model

The upper three equations in equation (10) are calculated numerically using the third-order Adams-Bashforth method as in the undrained case. Equation (S2) is calculated numerically using the method presented in Appendix B of Segall et al. (2010). In the following, we discuss the latter method. Near the shear zone, the discretization needs to be sufficiently fine to capture a steep

gradient of the pore fluid pressure. On the other hand, for a region far from the shear zone, the discretization does not need to be fine because the pore fluid pressure gradient is small. Thus, we use the following coordinate transformation between z and r (Segall et al., 2010):

$$z(r) = -c + e^{\mathrm{r}} \text{ or, equivalently, } r(z) = \ln(c + z).$$

We solve equation (S2) numerically in a new coordinate system using the Crank-Nicolson method. Specifically, we solve

$$\left\{1 + \frac{\gamma}{2} e^{-r_k}\left(e^{-(r_k-\delta)} + e^{-(r_k+\delta)}\right)\right\} p_k^{i+1}$$
$$= p_k^i + \frac{\gamma}{2} e^{-r_k} e^{-(r_k-\delta)}\left(p_{k-1}^i + p_{k-1}^{i+1}\right) - \frac{\gamma}{2} e^{-r_k} p_k^i \left(e^{-(r_k-\delta)} + e^{-(r_k+\delta)}\right), \qquad (S3)$$

where $\gamma = \Delta t/\Delta r^2$, $\delta = \Delta r/2$, and p_i^k is the value of the pore fluid pressure of the k-th grid in the new coordinate system at time step i. Δt andΔr represent increments in time and space, respectively. In this study, the number of grids is 35, and the starting position of the grid is $r(0) = \ln(0)$, $\Delta r = 0.3$, and $c = 10^{-4}$. Therefore, the grid farthest from the shear zone in the numerical calculation using c_{hyd}~10^{-1} m^2/s, T~12.4 h is approximately $z = 170$ m, while the grid farthest from the shear zone in the numerical calculation using c_{hyd}~10^{-3} m^2/s, T~12.4 h is approximately $z = 17$ m.

Text S4. The approximate solution for the tidal response of the drained model

The approximate solution for the drained model is derived in the same manner as in Section 3.1. The pore fluid pressure change due to fluid flow is represented as $p(z,t) = p_0 + \Delta p(z) e^{i\omega t}$, where $p(0,t)$ corresponds to the pore fluid pressure in the shear zone. The equations for the drained model corresponding to equations (13) and (14) for the undrained model are

$$\frac{\Delta \tilde{V}}{\tilde{V}_{pl}} = \frac{2\pi i}{\tilde{K}\tilde{V}_{pl} + 2\pi i C} |\Delta \tilde{S}(t)| \qquad (S4)$$

and

$$C = a - \frac{1}{1 + i\frac{T_\theta}{T}}\left(b - \mu_{pl}E_p\sqrt{2\pi i}\right), \text{respectively.} \qquad (S5)$$

The equations of the drained model corresponding to equations (17) and (18) for the undrained model are

$$\alpha = Re\left(\frac{2\pi i}{(\widetilde{K}\widetilde{V}_{pl} + 2\pi i C)\sigma_{eff}^0}\right) \qquad (S6)$$

and

$$\delta = arg\left(\frac{2\pi i}{\widetilde{K}\widetilde{V}_{pl} + 2\pi i C}\right), \text{respectively.} \qquad (S7)$$

Furthermore, by applying the argument from which equations (19) and (20) were derived for the drained model, the approximate solutions of α and δ can be expressed as

$$\alpha \sim Re\left\{\left(C\sigma_{eff}^0\right)^{-1}\right\} \qquad (S8)$$

and

$$\delta \sim arg\{C^{-1}\}, \qquad (S9)$$

respectively.

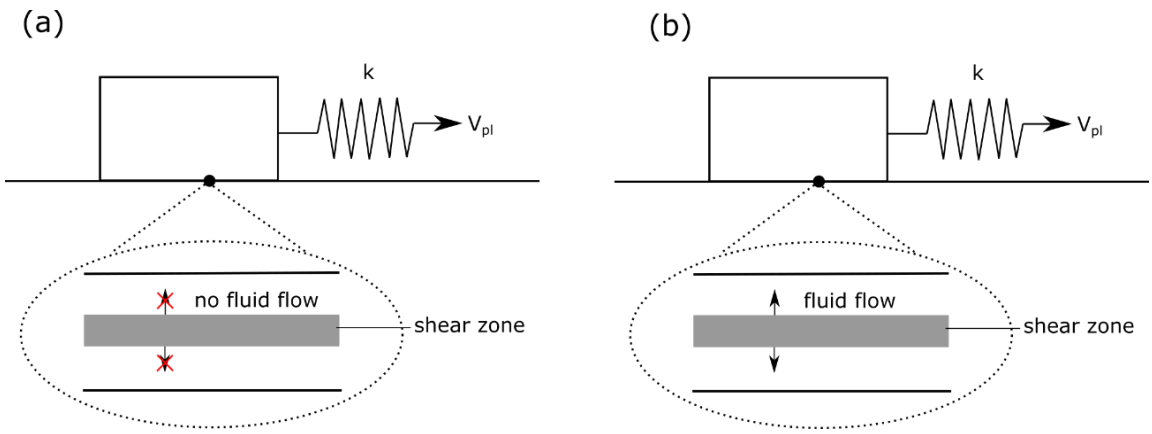

Figure S1. A schematic of the undrained (a) and drained (b) models. The difference between the two models is whether fluid flows outside the shear zone.

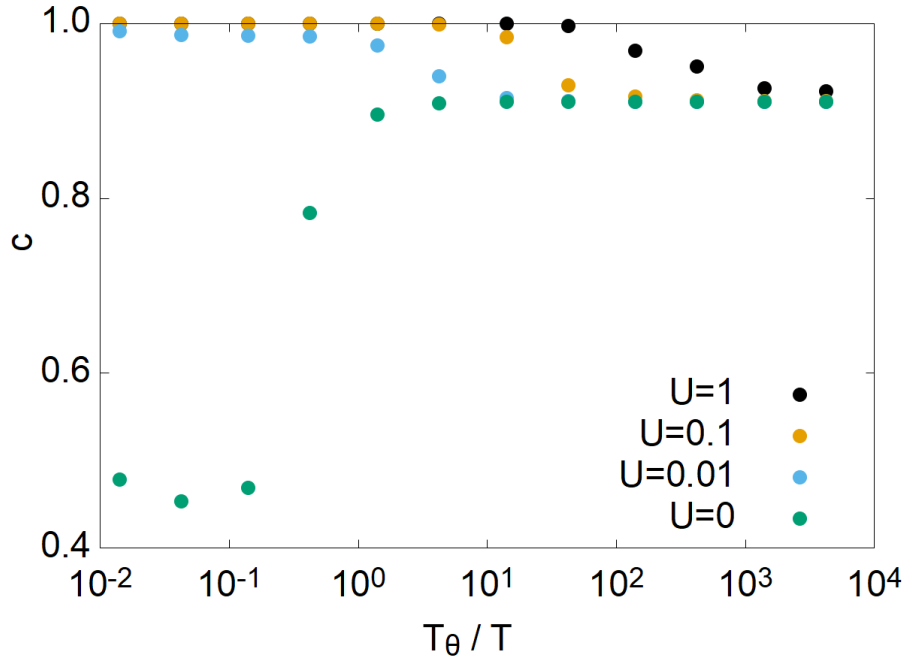

Figure S2. The numerical solution of ***c*** (dots). The differences in color represent differences in the dilatancy parameter ***U***.

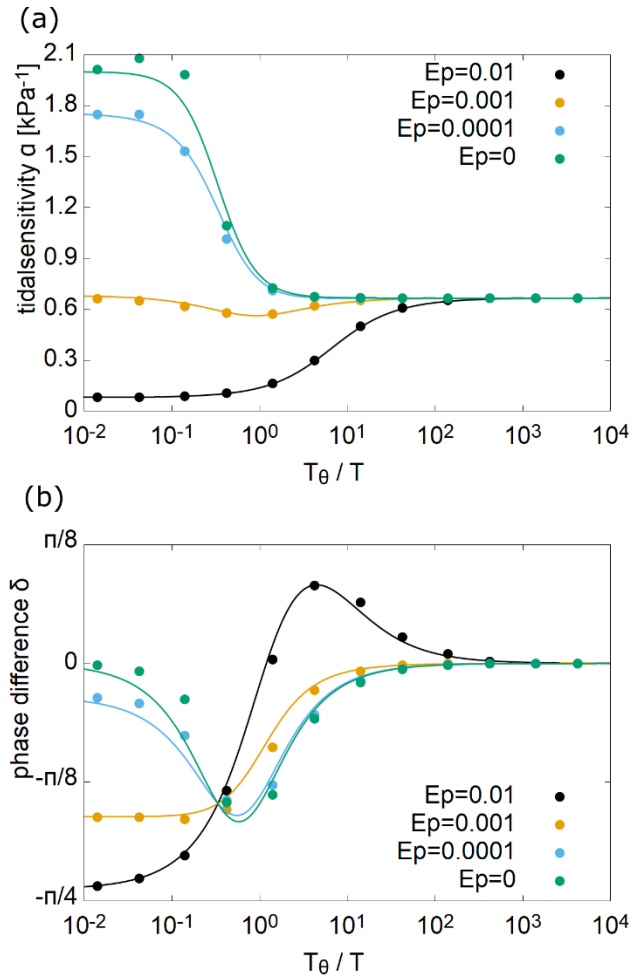

Figure S3. (a) The numerical solution of $\boldsymbol{\alpha}$ (dots) and the approximation solution (i.e., equation (S8)) (solid line). (b) The numerical solution of $\boldsymbol{\delta}$ (dots) and the approximation solution (i.e., equation (S9)) (solid line). The differences in color represent differences in the dilatancy parameter $\boldsymbol{E_p}$ for the drained model.

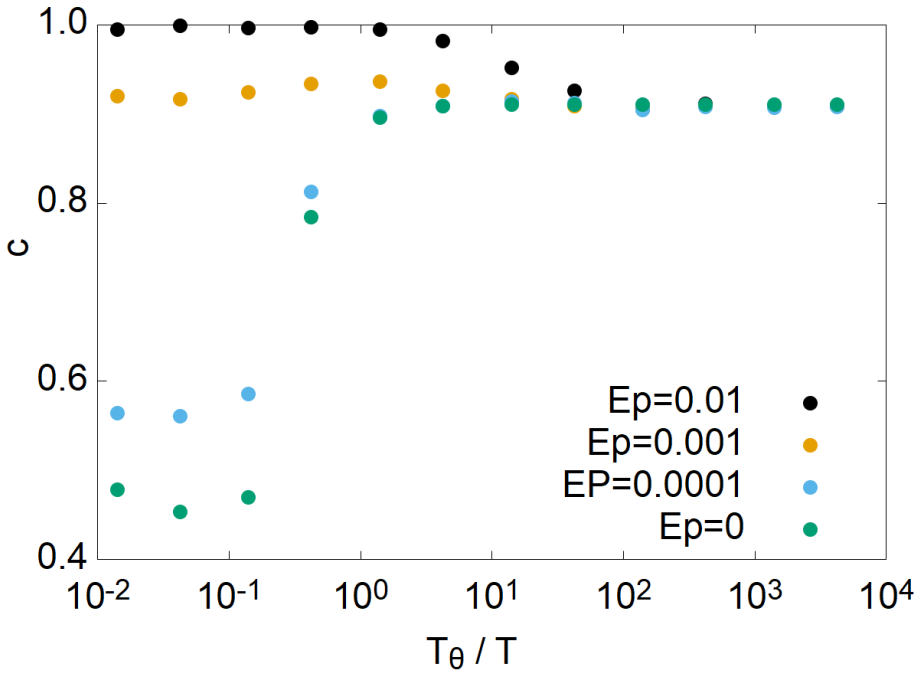

Figure S4. The numerical solution of $\boldsymbol{c}$ (dots). The differences in color represent differences in the dilatancy parameter $\boldsymbol{E_p}$ for the drained model.

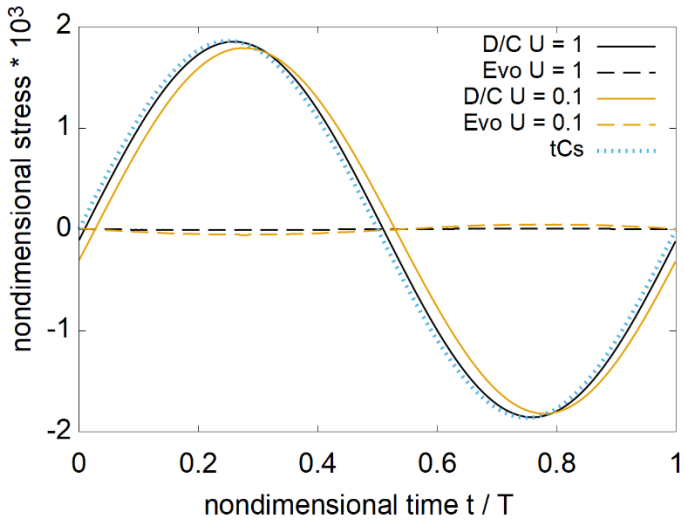

Figure S5. The time evolution of the dilatancy/compaction (D/C) term and the evolution (Evo) term for $U = 1$ and $U = 0.1$ (the variation from the time average over one tidal cycle is shown). The horizontal axis denotes the time normalized by the tidal period, and the values from 0 to 1 indicate one tidal cycle. The vertical axis denotes the tidal Coulomb stress (tCs) $\times 10^3$, normalized by the frictional strength σ_{eff}^0. The numerical solutions for $T_\theta/T = 14$ and $U = 1$ are shown in black, and those for $T_\theta/T = 4.2$ and $U = 0.1$ are shown in yellow. The amplitudes of the D/C term and tCs term are almost the same for $U = 0.1$ as well as $U = 1$. This means that the argument in Lines 407-414 in the body text can be applied to $U = 0.1$ as well as $U = 1$. Furthermore, the D/C term for $U = 0.1$ has a phase shift to the right of that for $U = 0.1$. Thus, $\beta(\ll \pi)$ at $U = 0.1$ is larger than $\beta(\ll \pi)$ at $U = 1$ ($\log(V/V_{pl}) \sim |\Delta S(t)| \sin(\beta/2) \cos(\omega t + (\pi - \beta)/2)$. See Appendix B). Since the tidal Coulomb stress peak corresponds to $\omega = \pi/2$, the larger β is, the smaller δ is. In other words, δ is smaller for $U = 0.1$ than for $U = 1$.

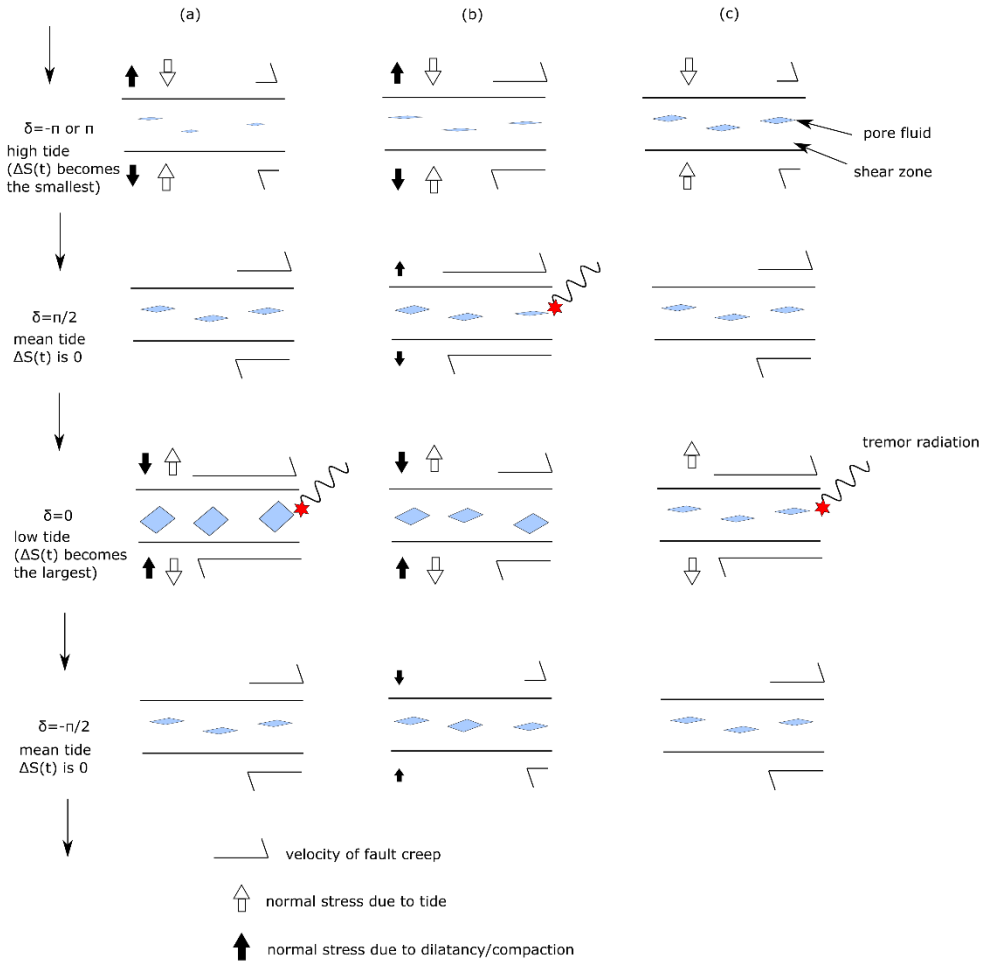

Figure S6. A schematic illustration of the relationship between the fault creep velocity and tide level when $U = 1$. For simplicity, only the normal stress change (white arrows) is represented. (a) Tidal modulation of fault creep when $T_\theta/T \ll 1$. Since the dilatancy/compaction effect (black arrows) decreases the amplitude of $\Delta S(t)$, the fault creep velocity reaches its maximum at $\delta \sim 0$. (b) Tidal modulation of fault creep when $T_\theta/T \ll 1$ and $T_\theta/T \gg |b - \mu_{pl}U|/a$. The sum of the normal stress due to the dilatancy/compaction effect and the tidal normal stress becomes the largest in the sense of enhancing fault slip at $\delta \sim \pi/2$. (c) Tidal modulation of fault creep when $T_\theta/T \gg |b - \mu_{pl}U|/a$. The dilatancy/compaction effect is negligible, and the fault creep velocity reaches its maximum at $\delta \sim 0$.

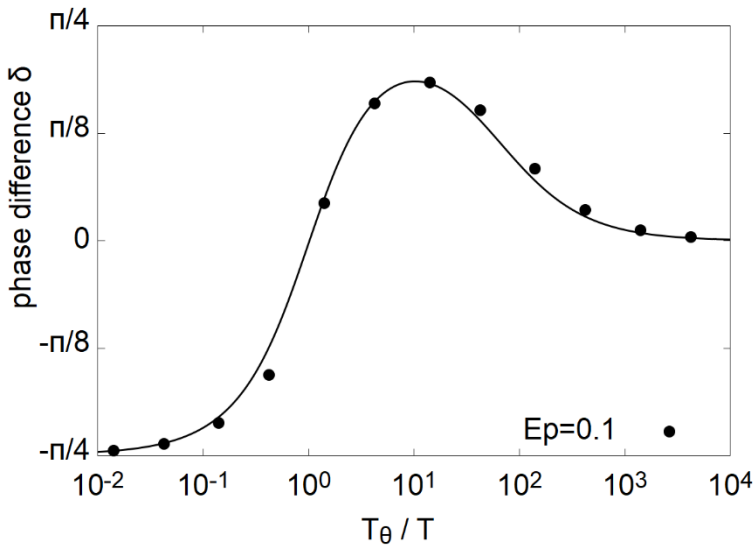

Figure S7. The dependence of T_θ/T on the phase difference at $E_p = 0.1$ The numerical solution of δ (dots) and the approximation solution (i.e., equation (S9)) (solid line). We see that the maximum phase difference is $\delta \sim \pi/6$ at $T_\theta/T \sim 10$, which cannot explain the observed phase difference of $\pi/2$.

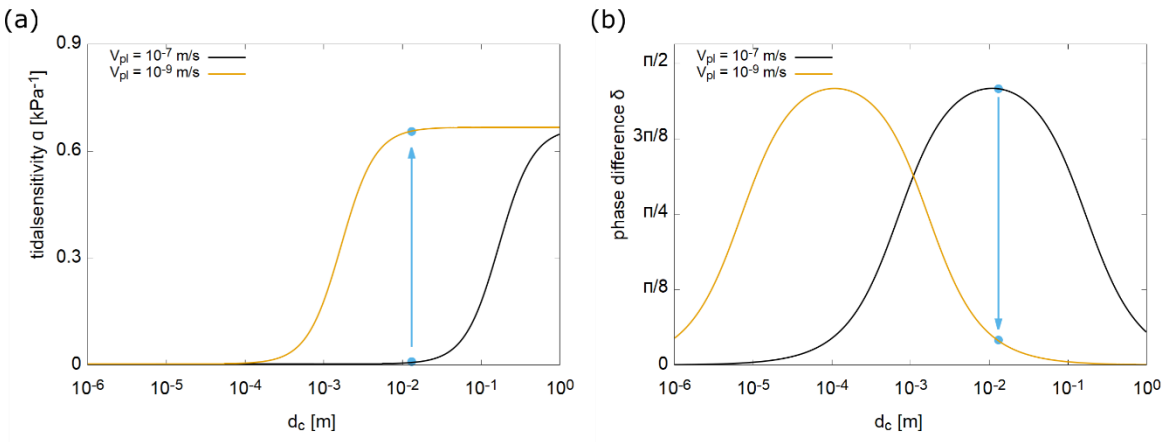

Figure S8. (a) The approximation solution of α (equation (19)) when $V_{pl} = 10^{-7}$ m/s (black) and 10^{-9} m/s (yellow). The horizontal axis denotes the critical slip distance d_c. The blue dots show that α for $d_c = 0.13$ m increases from $\lesssim 0.1$ to ~ 0.7 as V_{pl} decreases from 10^{-7} m/s to 10^{-9} m/s. (b) The same as in (a) but for the approximation solution of δ (equation (20)). The blue dots show that δ decreases from $\sim\pi/2$ to ~ 0 as V_{pl} decreases from 10^{-7} m/s to 10^{-9} m/s.